FULL PAPER

Tunable Nanochannels along Graphene Oxide/Polymer Core–Shell Nanosheets to Enhance Proton Conductivity

*Guangwei He, Chaoyi Chang, Mingzhao Xu, Shen Hu, Lingqiao Li, Jing Zhao, Zhen Li, Zongyu Li, Yongheng Yin, Mingyue Gang, Hong Wu, Xinlin Yang, Michael D. Guiver, and Zhongyi Jiang**

Simultaneous manipulation of topological and chemical structures to induce ionic nanochannel formation within solid electrolytes is a crucial but challenging task for the rational design of high-performance electrochemical devices including proton exchange membrane fuel cell. Herein, a novel generic approach is presented for the construction of tunable ion-conducting nanochannels via direct assembly of graphene oxide (GO)/poly(phosphonic acid) core–shell nanosheets prepared by surface-initiated precipitation polymerization. Using this simple and rapid approach to engineer GO/polymer nanosheets at the molecular-level, ordered and continuous nanochannels with interconnected hydrogen-bonded networks having a favorable water environment can be created. The resulting membranes exhibit proton conductivities up to 32 mS cm^{-1} at 51% relative humidity, surpassing state-of-the-art Nafion membrane and all previously reported GO-based materials.

1. Introduction

The demanding requirements for portable power sources with high energy density have triggered intensive efforts to improve membrane materials for proton exchange membrane fuel cells (PEMFCs).[1] However, the broad implementation of PEMFCs has been impeded partially by the current performance of proton exchange membranes (PEM), the core component of the device, because of insufficient proton conductivity under low humidity conditions.[2] Creation of ordered and continuous nanochannels for efficient ion-conduction is perceived as one of the most promising strategies to overcome this challenge.[3–5] Congregated ionic groups within the nanochannels lead to the formation of well-connected hydrogen-bonded networks or water structures, thus achieving high ion mobility even under an environment of minimal humidity.[4,6] Moreover, the cohesive hydrophobic matrix surrounding the nanochannels has strong intermolecular forces to suppress osmotic pressure-driven membrane swelling under hydration, accommodating the high ion exchange capacity (IEC).[7,8] The simultaneous augmentation of ion mobility and ion concentration (ionic conductivity ∝ ion mobility × ion concentration) is anticipated to bring about more efficient proton conduction.[9] Currently, a common approach to tailoring nanochannels has been accomplished by manipulating membrane nanophase-separation behavior through densely functionalized or block copolymer architecture, exploiting the spontaneous assembly of polymer morphology into ionic nanochannels (driven by the enthalpy of demixing of incompatible segments).[3,10] However, exercising precise control over the nanophase-separation process leading to nanochannels with long-range continuity is still a great challenge because nanophase-separation is markedly influenced by multiple factors such as the distribution, polarity, and rigidity of hydrophilic/hydrophobic segments, the IEC, and the processing conditions.[3,11] Furthermore, the polymer preparation may involve complex multistep synthesis to achieve the target architecture.[12]

To address these issues, we propose an alternative and more general approach involving the direct assembly of graphene oxide (GO)/polymer core–shell nanosheets into membranes via vacuum-assisted filtration, whereby efficient ion conduction occurs in the ionic nanochannels created between the GO nanosheets. The simple procedure should afford facile control over the topological structure and chemical structure of the ionic nanochannels through molecular-level engineering of the GO/polymer nanosheets. In terms of the topological structure, the GO/polymer nanosheets can be

Dr. G. He, J. Zhao, Z. Li, Z. Li, Y. Yin, M. Gang, Prof. H. Wu, Prof. X. Yang, Prof. M. D. Guiver, Prof. Z. Jiang
Collaborative Innovation Center of Chemical Science and Engineering
Tianjin 300072, P.R. China
E-mail: zhyjiang@tju.edu.cn

Dr. G. He, C. Chang, M. Xu, S. Hu, L. Li, J. Zhao, Z. Li, Z. Li, Y. Yin, M. Gang, Prof. H. Wu, Prof. Z. Jiang
Key Laboratory for Green Chemical Technology of Ministry of Education
School of Chemical Engineering and Technology
Tianjin University
Tianjin 300072, P. R. China

Prof. X. Yang
Key Laboratory of Functional Polymer Materials
Ministry of Education
Institute of Polymer Chemistry
Nankai University
Tianjin 300071, P.R. China

Prof. M. D. Guiver
State Key Laboratory of Engines
School of Mechanical Engineering
Tianjin University
Tianjin 300072, P.R. China

DOI: 10.1002/adfm.201503229

assembled into regularly stacked plate morphology, in which the orientated GO nanosheets generate an ordered and continuous nanochannel structure.[13] The nanochannel structure can be tuned by changing the GO interlayer spacing to ensure an optimum physical microenvironment for proton transport.[14] In terms of the chemical structure, the architecture and composition of GO-grafted polymers residing between the stacked plates can be tuned to ensure an appropriate chemical microenvironment for proton transport. In this regard, crosslinked phosphorylated polyelectrolyte may be a preferred choice, since amphoteric $-P=O(OH)_2$ groups are known to be superior proton carriers under low relative humidity (RH), and can afford dynamic hydrogen-bonded networks enabling fast hopping-type proton transport.[15,16] The crosslinked polyelectrolytes, which act as hydrogels, are well-known for their superior water retention properties. Hydrogels strongly absorb and retain a large amount of water via multiple interactions (hydrogen bonding, electrostatic interactions, and capillary forces), and are broadly applied in wound dressing, cosmetics, and agriculture for long-term moisture retention.[17,18] Therefore, crosslinked polyelectrolyte is sandwiched between GO nanosheets constrains swelling and should create an advantageous hydration environment along which fast vehicle-type proton transport could occur. The synergistic intensification of both hopping-type and vehicle-type proton transports, along with the tunable nanochannel structure, is expected to confer high proton conductivity under low RH.

In this study, we first report a surface-initiated precipitation polymerization method to synthesize multiple types of GO/polymer core–shell nanosheets, and then fabricate free-standing membranes via vacuum-assisted filtration assembly of GO/poly(vinylphosphonic acid-*co*-ethyleneglycol dimethacrylate) core–shell nanosheets. Precipitation polymerization is selected due to its unique capability of rapidly attaching polymer networks having tunable crosslinking degree onto the surfaces of diverse kinds of materials.[19,20] The GO-based membranes were evaluated in terms of proton conductivity, water uptake, swelling, methanol permeability, and mechanical properties. It is demonstrated that the GO-based membranes exhibit high proton conductivities up to 32 mS cm^{-1} at 51% RH primarily due to the construction of ordered and continuous nanochannels with well-tailored chemical structures.

2. Results and Discussion

2.1. Synthesis and Characterization of GO/Polymer Core–Shell Nanosheets

The synthetic approach to GO/polymer core–shell nanosheets is illustrated in **Scheme 1**. GO was modified with 3-(methacryloxy)propyltrimethoxysilane (MPS) to introduce readily polymerizable methacrylate groups.[21] Subsequently, covalently crosslinked polymer chains were grown on the surfaces of GO nanosheets, resulting in GO/polymer core–shell nanosheets. Methacrylic acid (MAA) was selected as the representative functional monomer to validate the precipitation polymerization in fabricating GO/polymer core–shell nanosheets. Fourier transform infrared (FTIR) spectra in **Figure 1** identify the functional groups in the GO-based nanosheets. In the GO sample, the characteristic absorption bands of GO are observed at 1728 cm^{-1} (C=O stretching vibrations), 1607 cm^{-1} (C=C stretching vibrations), 1229 cm^{-1} (C—O stretching vibrations in epoxy group), 1042 cm^{-1} (C—O stretching vibrations in C—OH groups), and 3475 cm^{-1} (O—H stretching vibrations).[22] The presence of these functional groups is further verified by X-ray photoelectron spectroscopy (XPS) (Figure S1, Supporting Information). The X-ray diffraction (XRD) pattern (Figure S1, Supporting Information) indicates that the *d*-spacing of GO nanosheets is 0.8 nm.[23] Upon grafting MPS, the GO-MPS sample shows absorption bands at 1016 and 1258 cm^{-1}, which are assigned to the stretching vibrations of the Si—O and C—O (in C—O—Si and O=C—O—C groups) groups, respectively.[24] The band at 1614 cm^{-1} (C=C stretching vibrations) becomes much stronger due to the introduction of more C=C bonds. The bands at 1029 and 1042 cm^{-1} (C—O stretching vibrations) observed in GO sample weaken or disappear, implying the reaction of C—OH and C—O—C groups in GO with MPS. The modification of MPS is essential to generate more reactive C=C bonds for the subsequent polymer attachment. We also attempted to functionalize the GO nanosheets without initial modification of GO by MPS, aiming at directly utilizing the C=C bonds of GO. However, the monomers tended to polymerize into microspheres instead of polymerizing on the GO nanosheets, as observed from transmission electron microscopy (TEM) (Figure S2, Supporting Information). These results collectively demonstrate the successful modification of MPS on the GO nanosheets. After the growth

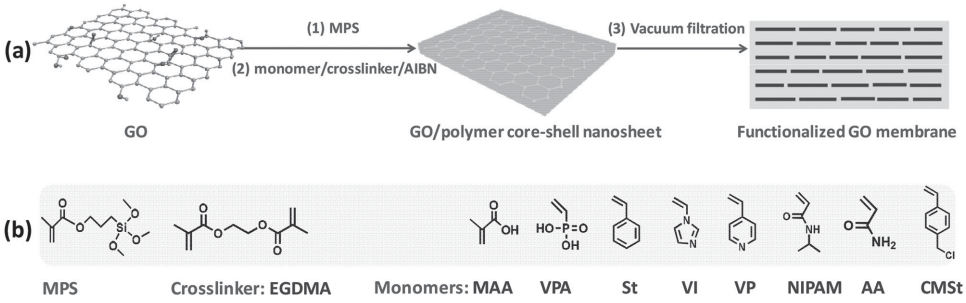

Scheme 1. a) Schematic illustration of the synthesis of GO/polymer core–shell nanosheets via surface-initiated precipitation polymerization of a variety of monomers, and the fabrication of functionalized GO membrane via vacuum filtration assembly of GO-poly(VPA-*co*-EGDMA) nanosheets; b) structures of MPS, crosslinker and monomers. EGDMA, VPA, St, VI, VP, NIPAM, AA, and CMSt are the abbreviations of ethylene glycol dimethacrylate, vinylphosphonic acid, styrene, vinylimidazole, 4-vinylpyridine, n-isopropyl-acrylamide, acrylamide, and 4-chloromethyl styrene, respectively.

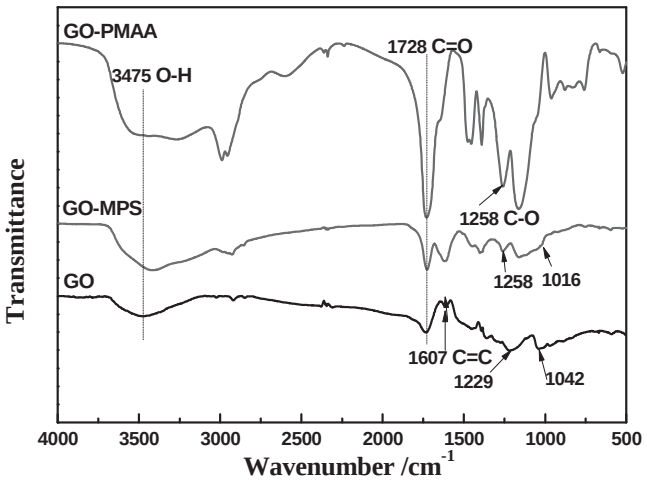

Figure 1. Comparative FTIR spectra of GO, GO-MPS, and GO-PMAA.

of poly(MAA-*co*-ethylene glycol dimethacrylate (EGDMA)) on GO-MPS nanosheets, the GO-*g*-poly(MAA-*co*-EGDMA) (GO-PMAA) sample exhibits stronger absorption bands at 1728 and 1265 cm^{-1}, which are attributed to the C=O and C—O stretching vibrations from the poly(MAA-co-EGDMA), respectively.

To acquire the morphological information of the GO-PMAA core–shell nanosheets, TEM and scanning electron microscope (SEM) characterization of GO-PMAA nanosheets was performed. The TEM images (Figure S3, Supporting Information) show that the black color on the nanosheets (on the top of the carbon film) darkens over polymerization time, indicating the growth of poly(MAA-*co*-EGDMA) network on the GO nanosheets over time. This result is further verified by the SEM images in **Figure 2**. In the initial stage of polymerization within 60 min, the nanosheet morphologies are not clearly detected because the nanosheets with small thickness tend to deform and stack.[25] After 60 min of polymerization, the lamellar morphologies are clearly observed. The thicknesses of the core–shell nanosheets at 80 and 100 min of polymerization are around 68 and 98 nm, respectively.

Thermogravimetric analysis (TGA) (Figure 2f) was performed to determine the mass ratios of PMAA in GO-PMAA and thermal properties of the GO-based nanosheets. Through analyzing the weight loss ratios of GO-MPS, GO-PMAA, and PMAA in the range of 125–780 °C of TGA curves, the PMAA ratios in GO-PMAA are calculated. The ratios of PMAA in GO-PMAA-20min, GO-PMAA-40min, GO-PMAA-60min, GO-PMAA-80min, GO-PMAA-100min reach 35.9, 74.3, 82.6, 87.4, and 91.8 wt%, respectively. These results indicate the exceptionally high efficiency of precipitation polymerization in fabricating GO/polymer core–shell nanosheets. Table S1 (Supporting Information) compares different "graft from" methods for grafting polymers onto GO or graphene nanosheets. In comparison with other "grafting from" approaches to modifying GO or graphene such as atomic transfer radical

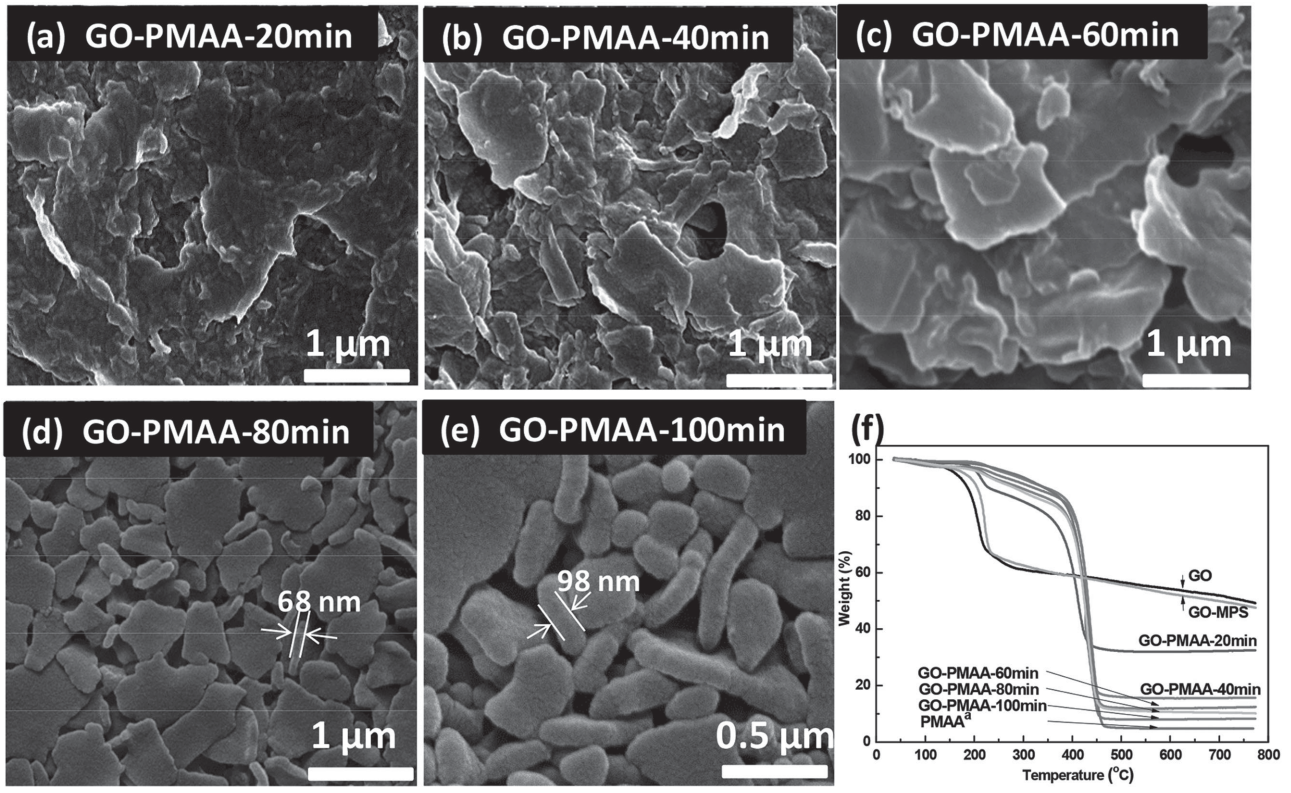

Figure 2. Surface images of GO-PMAA nanosheets observed by SEM: a) GO-PMAA-20min, b) GO-PMAA-40min, c) GO-PMAA-60min, d) GO-PMAA-80min, e) GO-PMAA-100min, f) Thermogravimetric Analysis (TGA) curves of GO, GO-MPS, GO-PMAA and PMAA, and "[a]" is cited from ref. [26]. After 100 min of polymerization, the thickness of GO-PMAA nanosheets reaches about 98 nm. Both the SEM images and TGA demonstrate the rapid attachment of polymers onto the surface of GO nanosheets over time.

polymerization,[27] reversible addition-fragmentation chain transfer polymerization,[28] cationic polymerization,[29] and free radical polymerization,[30] precipitation polymerization is more rapid and the corresponding graft yield is higher mainly due to two reasons: (i) the generated oligomers could precipitate out of the solvent (acetonitrile is a poor solvent for the oligomers) and be captured by the GO-PMAA nanosheets via covalent interactions. (ii) The concentrations of the reagents were increased by the distillation of solvent out of the reaction system.[19] All samples display two-stage weight loss, i.e., the evaporation of free and bound water in the first region (30–125 °C), and the decomposition of functional groups and polymer chains in the second region (125–780 °C). The GO and GO-MPS samples exhibit a typical weight loss in the region of 125–230 °C, corresponding to the decomposition of oxygen-containing groups.[29] With increasing reaction time, the TGA curves of the products (GO-PMAA) tend to be closer to the curve of pure polymer nanoparticles (PMMA sample). This phenomenon indicates the continuous attachment of polymers onto the surface of GO nanosheets over time, in agreement with the TEM and SEM observations.

The above result has demonstrated the feasibility, high efficiency, and simplicity of performing surface-initiated precipitation polymerization in yielding GO/polymer core–shell nanosheets. To confirm that this approach can be generally applied to other polymerizable vinyl monomers, we have employed a variety of typical monomers to functionalize GO nanosheets including vinylphosphonic acid (VPA), styrene (St), vinylimidazole (VI), 4-vinylpyridine (VP), n-isopropyl-acrylamide (NIPAM), acrylamide (AA), and 4-chloromethyl styrene (CMSt). The FTIR, TGA, and TEM characterization (Figures S4–S9, Supporting Information) demonstrates the successful functionalization of GO nanosheets using the above-mentioned monomers. The prepared GO/polymer nanosheets, with a variety of functional groups spanning acid, basic, hydrophilic, hydrophobic, thermal-sensitive, and pH-sensitive groups, may find applications across broad fields such as composite materials, ion exchange membranes, gas separation membrane, drug-delivery systems, and sensors.[31]

2.2. Fabrication and Properties of GO-poly(VPA-*co*-EGDMA) Membranes

2.2.1. Fabrication of GO-poly(VPA-co-EGDMA) Membranes

Besides corroborating the feasibility and universality of fabricating GO/polymer core–shell nanosheets using surface-initiated precipitation polymerization, another objective of this study is to implement the concept of creating tunable nanochannels for enhanced proton conductivity through assembling GO-poly(VPA-*co*-EGDMA) (PGO) nanosheets. The FTIR and XPS characterization in **Figure 3** verifies the successful synthesis of PGO nanosheets. The absorption bands at 1157 and 1103 cm^{-1} (Figure 3a) are attributed to the stretching vibrations of P—O bonds, and the band at 1358 cm^{-1} is ascribed to the stretching vibrations of P═O bonds.[32] The chemical composition is further determined by XPS. In the wide range XPS spectra (Figure 3b,d), the peaks at binding energies of 130.8 and 99.8 eV are assigned to P 2p and Si 2p, respectively. PGO-2 was synthesized by the same procedure and formula as PGO-1 but with

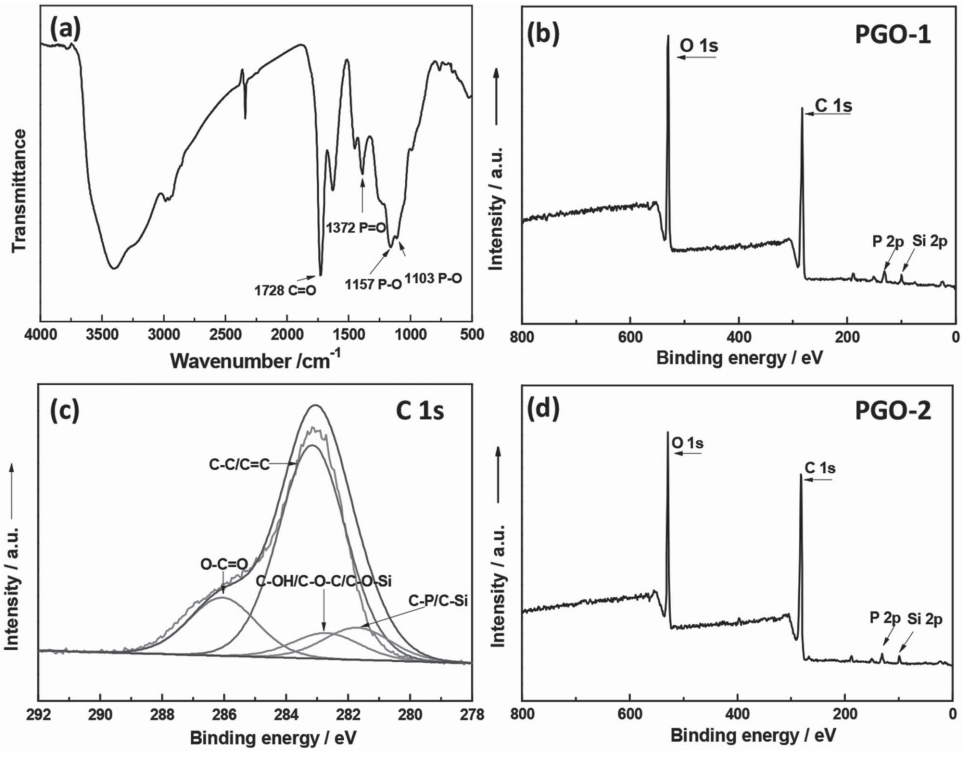

Figure 3. a) FTIR spectrum of PGO-1; b) wide region XPS spectrum of PGO-1; and c) deconvoluted XPS spectra in the C 1s region for PGO-1; d) wide region XPS spectrum of PGO-2.

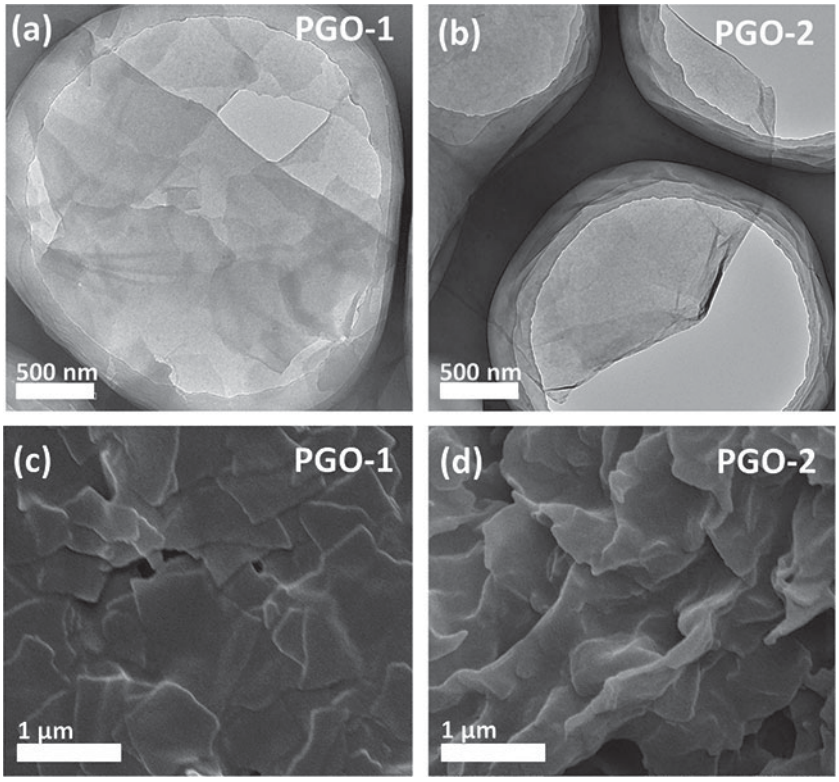

Figure 4. Surface images of PGO-1 and PGO-2 nanosheet samples observed by a,b) TEM and c,d) SEM.

shorter polymerization time. Thus, the major difference between them is the grafting ratio of polymer on GO. According to the peak area ratios, the P contents are calculated to be 6.69 wt% (Figure 3b) and 4.54 wt% (Figure 3d), which correlate with about 17.5 wt% (in PGO-1) and 11.9 wt% (in PGO-2) of $-P=O(OH)_2$ groups, respectively. The elemental ratios may deviate from the true value because only the surface composition (<10 nm depth) can be probed by XPS. The C 1s XPS spectra of PGO-1 (Figure 3c) show four peaks at binding energies of 283.15, 286.05, 282.7, and 281.7 eV, which are assigned to C—C/C=C (64.75%), O—C=O (17.67%), C—P/C—Si (7.84%) and C—OH/C—O—C/C—O—Si (9.74%), respectively.[33,34] The TEM and SEM images in **Figure 4** exhibit 2D morphologies of the PGO nanosheets.

The dispersion and filtration of the nanosheets via a vacuum-assisted filtration method[35] generated freestanding PGO membranes (Figure S10, Supporting Information). The SEM images in **Figure 5** show the cross-sections of the PGO membranes, revealing regularly stacked microstructure with a layer-by-layer morphology. This lamellar microstructure is also observed in other GO membranes prepared by filtration method.[36] The PGO nanosheets tend to orientate in the in-plane direction. The orderly distributed GO nanosheets render interconnected nanostructures with long-range continuity at micrometer length scale, which are advantageous to afford well-connected hydrogen-bonded networks and thus high proton conductivity. However, the PGO membranes have the drawback that the in-plane orientated PGO nanosheets confer highly tortuous proton-transport nanochannels. The TGA curves of the PGO membranes (Figure 5b) present two distinct weight losses at about 210 and 350 °C, respectively, corresponding to the removal of oxygen-containing groups of GO and the decomposition of the polymers in PGO membranes. According to the weight losses of GO-MPS nanosheets, PGO membranes, and poly(VPA-*co*-EGDMA), the poly(VPA-*co*-EGDMA) mass ratios in PGO-1 and PGO-2 membranes are calculated to be 44.6 and 31.8 wt%, respectively. **Figure 6** shows the XRD patterns of PGO-1, PGO-2, and GO membranes in the dry and wet states, indicating the tunable feature of the *d*-spacing within PGO membranes. The *d*-spacing of PGO-1, PGO-2, and GO membranes in the wet state are 1.43, 1.33, and 1.2 nm, respectively. The variation of *d*-spacing is in accordance with the change of grafting ratio of polymers on GO, that is, higher polymer content residing between the GO nanosheets renders larger *d*-spacing. The *d*-spacing in the wet state is larger than that in the dry state due to the swelling of the polymers.

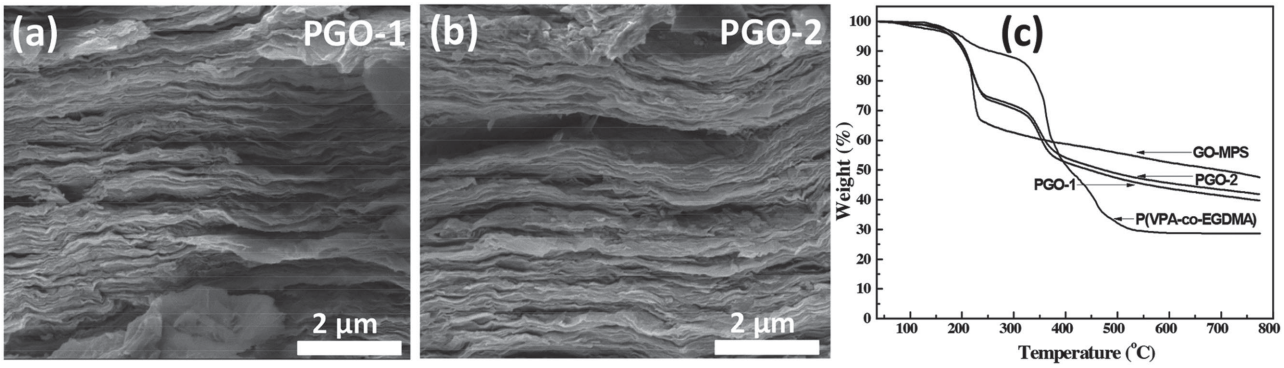

Figure 5. a,b) SEM images of cross-section morphologies of PGO-1 and PGO-2 membranes. The membranes show orderly stacked lamellar microstructure, which provides desirable nanochannel morphology with long-range continuity for proton transport; c) TGA curves of GO-MPS, PGO-1 and PGO-2 membranes, and poly(VPA-*co*-EGDMA).

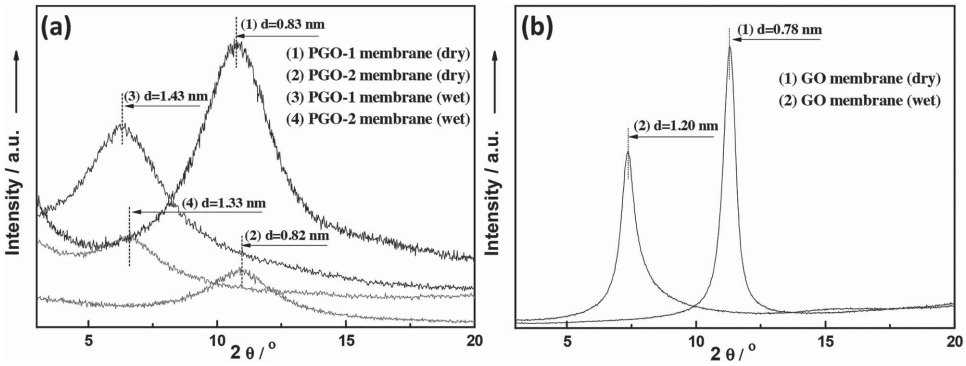

Figure 6. XRD patterns of a) PGO-1 and PGO-2 membranes and b) GO membrane in the dry and wet states (immersed in water for 24 h before measurement) at room temperature.

2.2.2. Water Uptake and Dimensional Change of the Membranes

Water uptake is a key parameter to gain insight into the mode of proton transport due to the fact that water molecules are involved in both the vehicle mechanism and Grotthuss mechanism.[16] **Table 1** shows that the water uptake of PGO-1 membrane is 47.5% at 30 °C, which is double that of Nafion 117. The PGO-2 displays a lower water uptake due to the decreased IEC. The water uptakes of PGO-1 and PGO-2 membranes correspond to about 10.6 and 9.6 water molecules per $-P{=}O(OH)_2$ group ($[H_2O]/[P{=}O(OH)_2]$), respectively. These results indicate that the membranes possess sufficiently high water uptake, which is essential to the formation of percolated water structures for fast proton transport.

Dimensional change was evaluated by the swelling ratio of PGO membrane in water. For PGO-1 membrane, the swelling ratio in the through-plane direction is 27.8%, while the swelling ratio in the in-plane direction is only 2.5%. Such a significant anisotropic swelling behavior originates from the fact that the nanosheets in membrane tend to orientate in the in-plane direction (observed by SEM), which markedly suppresses the swelling of membrane in the in-plane direction. This anisotropic behavior is frequently observed in multiblock copolymer membranes because of the in-plane orientation of ionic nanochannels in membranes.[37,38] It should be mentioned that the small in-plane swelling is beneficial in preparing membrane electrode assemblies because excessive in-plane swelling can lead to the delamination of catalyst layer.

2.2.3. Mechanical Stability of the Membranes

The stress–strain curves in Figure S11 (Supporting Information) show that the PGO-1 membrane exhibits tensile strength of 29.1 MPa, Young's modulus of 0.73 GPa, and elongation at break of 16.4% in the dry state. The good mechanical properties are due to the abundant physical interactions between PGO nanosheets. The mechanical properties could rival those of composite or aromatic ionomer membranes reported in the literature.[7,39]

2.2.4. Proton Conductivity of the Membranes

Proton conductivity is the performance-determining parameter in PEMFC. As listed in Table 1, the proton conductivity of PGO membrane exhibits a positive correlation with the IEC, and the conductivity reaches 71 mS cm^{-1} at IEC of 2.5 mmol g^{-1} under 30 °C and 100% RH. Under fully hydrated conditions, sulfonated membranes usually show a significantly higher conductivity than that of phosphonated membranes mainly because the sulfonated acid group (strong acid) is more easily dissociated, allowing a high concentration of free protons.[16,37] However, the conductivity of PGO-1 membrane is comparable to that of the benchmark membrane (Nafion 117). Moreover, the conductivity is higher when compared with either state-of-the-art phosphonated membranes[40,41] or GO-based materials[42] (Table S2, Supporting Information). For example, the PGO-1 membrane shows conductivity nearly 20 times higher than those of GO and GO-MPS membranes, indicating the importance of introducing phosphonated polymers. The phosphonated membrane with poly(VPA) brushes shows a conductivity of 66 mS cm^{-1} at a remarkably high IEC of 5.3 mmol g^{-1} (water uptake = 125%), and the conductivity decreases to 17 mS cm^{-1} with decreasing the IEC to 2.9 mmol g^{-1} (water uptake = 31%).[41] This means that the PGO-1 membrane achieves a significantly elevated conductivity at a lower IEC (2.5 mmol g^{-1}), indicating that the ion

Table 1. IEC, dimensional swelling, water uptake, proton conductivity of the membranes.

Membrane	IEC	Swelling [%]		Water uptake[b)] [%]		Proton conductivity[a)]
	[mmol P per gram]	(in plane)[a)]	(through plane)[a)]	30 °C	80 °C	[mS cm^{-1}]
PGO-1	2.5	2.5	27.8	47.5	73.2	71
PGO-2	1.4	1.9	16.4	24.3	36.7	42
Nafion 117	0.9	9.8	11.3	18.6	25.6	86

[a)]Measured at 30 °C in water; [b)]Measured at 30 and 80 °C in water.

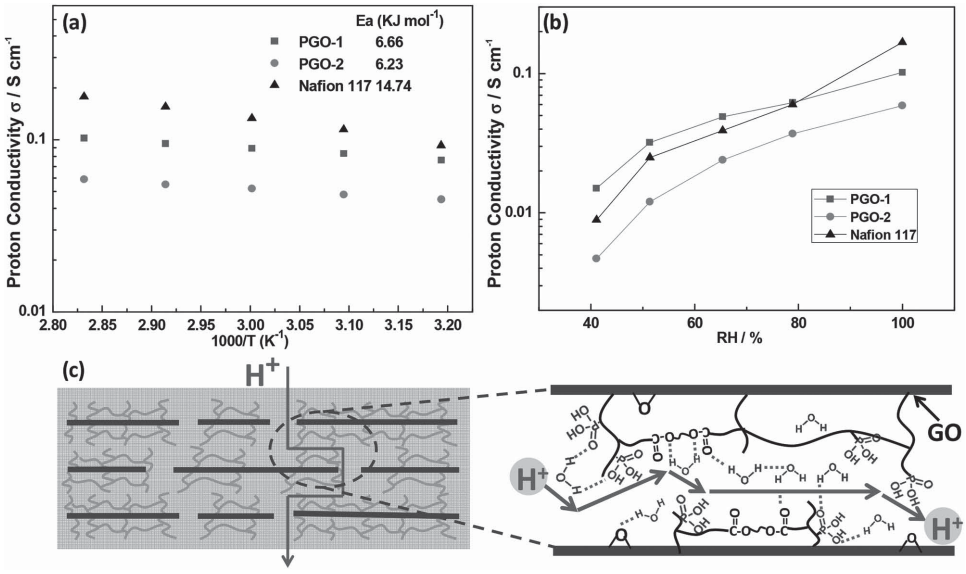

Figure 7. Proton conductivity of PGO and Nafion 117 membranes a) as a function of temperature at 100% RH and b) as a function of humidity at 80 °C. c) Illustration of proton transport along the hydrogen-bonded network within the nanochannels.

mobility is much higher.[37] This high ion mobility is mainly due to the reason that the PGO-1 membrane possesses a more efficient organization of proton carriers.[43] Extensive long-range ionic nanochannels are believed to be created on the functionalized GO nanosheets having continuous geometric structures.[44] **Figure 7**a shows the proton conductivity of PGO and Nafion 117 membrane in the range of 40–80 °C. The conductivities increase with increasing temperature because proton transport is a thermally activated process. The conductivity of PGO-1 membrane achieves 102 mS cm^{-1} at 80 °C. The calculated activation energy (E_a) of the PGO-1 membrane is 6.65 kJ mol^{-1}, 45.23% of the E_a of Nafion 117 (14.7 kJ mol^{-1}), implying the creation of lower-energy-barrier pathways for proton transport.[18]

Figure 7b plots the proton conductivity as a function of humidity at 80 °C. The dependence of conductivity on humidity for the PGO membrane is lower than that for Nafion 117 membrane. At 51% RH, the conductivity of PGO-1 membrane is 32 mS cm^{-1}, 28% higher than the value of Nafion 117 membrane (25 mS cm^{-1}). To the best of our knowledge, this is the highest conductivity for GO-based materials reported to date. Such high conductivity at low RH is attributed to the following three reasons: (i) the conductivity of phosphonated membrane has a weaker dependence on humidity compared with that of sulfonated membrane.[45] Phosphonic acid group is amphoteric, and it can act as both proton donor and proton acceptor. Dynamic hydrogen bonded networks can be formed among $-PO_3H_2$ groups, allowing proton transport even under anhydrous conditions;[33,46] (ii) the crosslinked polyelectrolyte behaves as a hydrogel and is expected to provide excellent water retention properties under low RH;[47] (iii) the crosslinked polyelectrolyte between GO layers possesses a high local concentration of $-P=O(OH)_2$ groups (2.5 mmol P per gram) as well as other hydrophilic groups such as —COOH, —C=O, and glycol groups. These abundant functional groups interact with the absorbed water to create well-connected hydrogen-bonded networks (continuous ionic nanochannels) between the orderly distributed GO layers, as illustrated in Figure 7c. It is noteworthy that this is the first study on phosphorylated GO for proton transport.

2.2.5. Methanol Permeability of the Membranes

In order to explore the application potential of PGO membrane in direct methanol fuel cell (DMFC), the methanol permeability was measured at 30 °C. Membranes for DMFC must simultaneously have high proton conductivity and low methanol permeability. However, proton conductivity and methanol permeability are strongly coupled, and it remains a great challenge to fabricate membranes having both favorable conductivity and methanol-barrier properties.[48] For the permeability measurement using 2 M methanol (**Figure 8**), the PGO-1 and PGO-2 membranes display methanol permeability of 4.3×10^{-7} and 2.3×10^{-7} cm^2 s^{-1}, respectively, which are lower than that

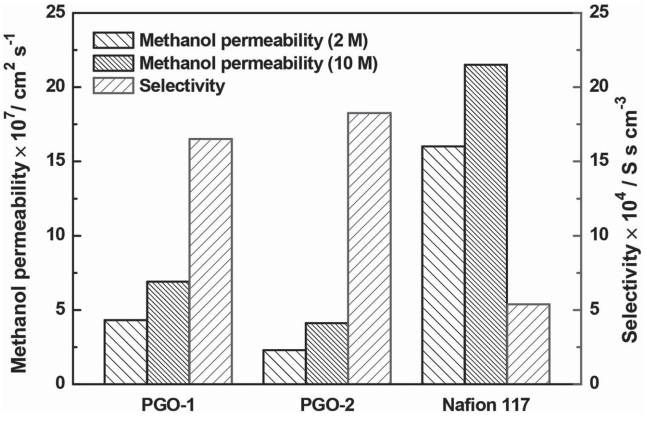

Figure 8. Methanol permeability (in 2 M and 10 M methanol solution) and selectivity of PGO and Nafion 117 membranes. The selectivity is calculated based on the proton conductivity (30 °C in water) and the methanol permeability in 2 M methanol solution.

of Nafion 117 membrane (1.6×10^{-6} cm^2 s^{-1}). This is attributed to the fact that the in-plane orientation of GO nanosheets (impermeable to methanol) extends the pathway for methanol diffusion, and that the crosslinked polymer networks are unfavorable for methanol diffusion.[20] The PGO membranes also exhibit low methanol permeability (Figure 8) under high methanol concentration (10 M), indicating their potential for application in high concentration DMFC. The selectivity (proton conductivity/methanol permeability) is a more comprehensive parameter to evaluate the potential performance of the membrane in DMFC.[49] The selectivity of PGO-1 membrane (Figure 8) is 1.65×10^5 S s cm^{-3}, which is 3.07 times of that of Nafion 117 membrane (5.38×10^4 S s cm^{-3}). Such a high selectivity is anticipated to be beneficial for high-performance DMFC.

As a proof-of-principle study, this work demonstrates the construction of tunable nanochannels within membrane via directly assembling GO/polymer nanosheets. The formulation enables independent control over the topological structure and chemical structure of nanochannels. This is the first exploitation of constructing ionic nanochannels with tunable features using functionalized GO, offering an insight into the rational design of high-performance solid electrolyte for practical applications. Further work will be focused on evaluating the fuel cell performance and long-term stability of the membrane.

3. Conclusion

Herein, we reported a rapid, simple, and general approach for the synthesis of GO/polymer core–shell nanosheets via surface-initiated precipitation polymerization. A remarkably high graft yield of 94% was achieved within only 1.67 h. The high graft efficiency, coupled with the compatibility with various monomers and insensitivity to oxygen, water, and polymerization inhibitor, makes this approach broadly attractive to other fields.

Subsequently, we fabricated GO-based membranes via vacuum-assisted filtration assembly using GO/poly(VPA-*co*-EGDMA) core–shell nanosheets as building blocks. At a RH of 51%, the proton conductivity of PGO-1 membrane reaches 32 mS cm^{-1}, surpassing the performance of all GO-based materials reported to date. Such a high conductivity is attributed to the construction of ordered and continuous nanochannels with well-tailored chemical structures. The regularly distributed GO nanosheets provide the nanochannel structure with long-range continuity (observed by SEM) ensuring appropriate physical microenvironment, while the poly(VPA-*co*-EGDMA) confers well-connected hydrogen-bonded network and excellent water retention ensuring appropriate chemical microenvironment, resulting in the simultaneous intensification of hopping-type and vehicle-type proton transport. Considering the tunable feature and high performance, the proposed straightforward strategy of constructing nanochannels may become a benchmark for molecular-level design of next-generation PEMs.

4. Experimental Section

Materials: GO (thickness 0.55–1.2 nm, diameter 0.5–3 μm) was purchased from Chengdu Organic Chemicals Co. Ltd., Chinese Academy of Sciences. MPS, EGDMA, and styrene (St) were purchased from Alfa Aesar (China) and used as received. 2, 2′-Azoisobutyronitrile (AIBN) and acrylamide were purchased from Aladdin (China) and used without further purification. MAA, VPA, VI, NIPAM, VP, CMSt were purchased from J & K Chemical Ltd. (China) and used as received. All other reagents were reagent grade and used without further purification. De-ionized water was utilized in the entire experiment.

Synthesis of GO/Polymer Nanosheets: GO was modified with MPS according to our previous work.[26] 100 mg of GO was dispersed in 50 mL of ethanol with ultrasonic radiation. After adding 0.2 mL of MPS, the solution was stirred for 48 h at 50 °C. The resultant MPS-modified GO (MPS-GO) was purified by three cycles of centrifugation/redispersion using ethanol as solvent.

Multiple types of GO/polymer core–shell nanosheets were prepared through surface-initiated precipitation polymerization using MPS-GO as template.[19,50] A typical procedure for the fabrication of GO/poly(MAA-*co*-EGDMA) (GO-PMAA) nanosheets was described below. 20 mg of MPS-GO, 0.5 mL of MAA, 0.5 mL EGDMA, and 0.02 g of AIBN (2 wt% relative to the weight of [MAA+EGDMA]) were dissolved in 80 mL of acetonitrile. This solution was heated to boiling state from room temperature within 10 min, and then the solvent was kept being distilled out of the reaction system. After a predetermined reaction time (20–100 min), the resulting core–shell nanosheets were purified by centrifugation and redispersion. The polymer grafting ratio can be controlled by varying three parameters: (i) the (monomer+crosslinker)/MPS-GO feed ratio; (ii) the concentrations of monomer and crosslinker in acetonitrile; and (iii) the reaction time. The crosslinking degree can be controlled by varying the crosslinker/monomer ratio. Finally, the GO/polymer nanosheets with different kinds of compositions were obtained after drying in a vacuum oven. PGO nanosheets were prepared by a similar method to GO-PMAA except for the following differences: 20 mg of MPS-GO, 0.3 mL of VPA, 0.15 mL EGDMA, and 0.009 g of AIBN were dissolved in 80 mL of acetonitrile. The polymerization was allowed to proceed for 40 and 60 min, resulting in PGO-2 and PGO-1 nanosheets, respectively. Poly(VPA-co-EGDMA) microsphere was synthesized to determine the mass ratio of polymer in PGO membrane, according to the method reported in our previous study.[26]

Membrane Preparation Via Vacuum Assisted Assembly Method: 60 mg of PGO nanosheets were dispersed in 120 mL of water under ultrasonic irradiation for 60 min. The suspension was then filtered through a commercial microfiltration membrane (polyether sulfone membrane with a pore diameter of 220 nm) under vacuum for about 24 h. The resulting membrane was then dried at room temperature for 24 h and at 60 °C for 12 h. For comparison, the GO membrane was prepared though the filtration of GO aqueous dispersion (0.5 mg mL^{-1}) by the same method as the PGO membrane.

Characterization: The morphology of the GO/polymer nanosheets was observed by transmission electron microscopy (TEM, Tecnai G2 20 S-TWIN) and field emission scanning electron microscope (FESEM, Nanosem 430). Cross-section morphology of the membrane was imaged by FESEM after the membrane being freeze-fractured in liquid nitrogen and then sputter-coated with a thin gold layer. The samples of GO-based nanosheets for TEM and SEM characterization were prepared through dropping their dispersions on carbon films and conducting adhesives, respectively, followed by drying. FTIR spectra of the samples were measured by a BRUKER Vertex 70 FTIR spectrometer equipped with a horizontal attenuated transmission accessory. The chemical compositions of GO or PGO were determined using XPS (Kratos Axis Ultra DLD) with a monochromatic Al Kα source and a charge neutralizer. Wide-angle XRD was performed to detect the crystallization property of GO using a D/MAX-2500 X-ray diffractometer (CuK α). TGA was performed using a thermogravimetric analyzer (NETZSCH-TG209 F3) over a temperature range of 40–800 °C at a heating rate of 10 °C min^{-1} under nitrogen atmosphere.

Measurement of Water Uptake, Dimensional Swelling, and IEC: Rectangular samples were dehydrated till constant weight and the weight (W_{dry}), length (L_{dry}), and thickness (T_{dry}) were tested. Subsequently, the samples were immersed in water at a defined temperature until full hydration and the weight (W_{wet}), length (L_{wet}), and thickness (T_{wet})

were tested. The measurements were repeated three times to obtain an average value. The water uptake, length swelling, and thickness swelling were respectively calculated by the equations: water uptake (%) = $(W_{wet} - W_{dry})/W_{dry} \times 100$, ΔL (%) = $(L_{wet} - L_{dry})/L_{dry} \times 100$ and ΔT (%) = $(T_{wet} - T_{dry})/T_{dry} \times 100$. The IEC was measured through back titration method. The sample was immersed in 0.01 M of NaOH for 48 h, and then the remained amount of NaOH was titrated. The IEC (mmol P per gram) was calculated by $M_{NaOH}/(2W_{dry})$, where M_{NaOH} is the molar weight of the NaOH consumed by the sample.

Measurement of Proton Conductivity, Methanol Permeability and Mechanical Property: The membrane resistance (R) was tested by two-point probe alternating current (AC) impedance spectroscopy with a frequency range of 10^5–1 Hz using an electrode system connected with frequency response analyzer (FRA, Compactstat, IVIUM Tech.). In-plane proton conductivity under 100% RH was tested in a temperature-controlled water-bath chamber, and the sample was probed by two parallel platinum electrodes. Proton conductivity under low RH at 80 °C was tested in a temperature-controlled chamber where the humidity was controlled by saturated salt solution. The salts employed to control humidity were as follows: K_2CO_3 (41.1%), NaBr (51.4%), $NaNO_3$ (65.4%), and KCl (78.9%).[51] Proton conductivity was calculated according to the relationship: $\sigma = l/AR$, where R is the resistance, A is the cross-section of the sample, and l is the length between the electrodes. The methanol permeability was measured using a diffusion cell, in which the methanol solution (2 M and 10 M) permeates through the PGO membrane into the water compartment. The measurement method was described in detail in our previous study.[52] Mechanical properties of dry membrane samples were tested by an electronic tensile machine (WDW-2, Yangzhou Zhongke Measuring Apparatus Co., China) at a stretching rate of 1 mm min^{-1} at room temperature.[26]

Supporting Information

Supporting Information is available from the Wiley Online Library or from the author.

Acknowledgements

The authors thank the financial support from the National Science Fund for Distinguished Young Scholars (21125627), and the Program of Introducing Talents of Discipline to Universities (B06006).

Received: August 3, 2015
Revised: September 11, 2015
Published online: November 17, 2015

[1] H. Zhang, P. K. Shen, *Chem. Rev.* **2012**, *112*, 2780.
[2] C. H. Park, C. H. Lee, M. D. Guiver, Y. M. Lee, *Prog. Polym. Sci.* **2011**, *36*, 1443.
[3] N. Li, M. D. Guiver, *Macromolecules* **2014**, *47*, 2175.
[4] N. Li, C. Wang, S. Y. Lee, C. H. Park, Y. M. Lee, M. D. Guiver, *Angew. Chem. Int. Ed.* **2011**, *50*, 9158.
[5] a) S. Y. Lee, N. R. Kang, D. W. Shin, C. H. Lee, K.-S. Lee, M. D. Guiver, N. Li, Y. M. Lee, *Energy Environ. Sci.* **2012**, *5*, 9795; b) Y. Yao, Z. Lin, Y. Li, M. Alcoutlabi, H. Hamouda, X. Zhang, *Adv. Energy Mater.* **2011**, *1*, 1133; c) Y. Chang, G. F. Brunello, J. Fuller, M. L. Disabb-Miller, M. E. Hawley, Y. S. Kim, M. A. Hickner, S. S. Jang, C. Bae, *Polym. Chem.* **2013**, *4*, 272.
[6] C. C. D. Araujo, K. D. Kreuer, M. Schuster, G. Portale, H. Mendil-Jakani, G. Gebel, J. Maier, *Phys. Chem. Chem. Phys.* **2009**, *11*, 3305.
[7] N. Li, S. Y. Lee, Y.-L. Liu, Y. M. Lee, M. D. Guiver, *Energy Environ. Sci.* **2012**, *5*, 5346.
[8] G. Titvinidze, K.-D. Kreuer, M. Schuster, C. C. de Araujo, J. P. Melchior, W. H. Meyer, *Adv. Funct. Mater.* **2012**, *22*, 4456.
[9] G. He, Z. Li, J. Zhao, S. Wang, H. Wu, M. D. Guiver, Z. Jiang, *Adv. Mater.* **2015**, *27*, 5280.
[10] S. Takamuku, P. Jannasch, *Adv. Energy Mater.* **2012**, *2*, 129.
[11] Y. A. Elabd, M. A. Hickner, *Macromolecules* **2011**, *44*, 1.
[12] S. Takamuku, P. Jannasch, *Macromolecules* **2012**, *45*, 6538.
[13] a) B. Mi, *Science* **2014**, *343*, 740; b) R. R. Nair, H. A. Wu, P. N. Jayaram, I. V. Grigorieva, A. K. Geim, *Science* **2012**, *335*, 442.
[14] a) H. Huang, Z. Song, N. Wei, L. Shi, Y. Mao, Y. Ying, L. Sun, Z. Xu, X. Peng, *Nat. Commun.* **2013**, *4*, 2979; b) Y. H. Yang, L. Bolling, M. A. Priolo, J. C. Grunlan, *Adv. Mater.* **2013**, *25*, 503.
[15] A. Sannigrahi, S. Takamuku, P. Jannasch, *Polym. Chem.* **2013**, *4*, 4207.
[16] K.-D. Kreuer, *Chem. Mater.* **2014**, *26*, 361.
[17] a) T.-Y. Liu, S.-Y. Chen, Y.-L. Lin, D.-M. Liu, *Langmuir* **2006**, *22*, 9740; b) J. Wang, H. Zhang, X. Yang, S. Jiang, W. Lv, Z. Jiang, S. Z. Qiao, *Adv. Funct. Mater.* **2011**, *21*, 971.
[18] J. Wang, X. Yue, Z. Zhang, Z. Yang, Y. Li, H. Zhang, X. Yang, H. Wu, Z. Jiang, *Adv. Funct. Mater.* **2012**, *22*, 4539.
[19] G. L. Li, H. Mohwald, D. G. Shchukin, *Chem. Soc. Rev.* **2013**, *42*, 3628.
[20] G. He, Y. Li, Z. Li, L. Nie, H. Wu, X. Yang, Y. Zhao, Z. Jiang, *J. Power Sources* **2014**, *248*, 951.
[21] G. Li, Z. Zheng, H. Möhwald, D. G. Shchukin, *ACS Nano* **2013**, *7*, 2470.
[22] B. T. McGrail, B. J. Rodier, E. Pentzer, *Chem. Mater.* **2014**, *26*, 5806.
[23] Y. Tian, Y. Cao, Y. Wang, W. Yang, J. Feng, *Adv. Mater.* **2013**, *25*, 2980.
[24] X. Ou, L. Jiang, P. Chen, M. Zhu, W. Hu, M. Liu, J. Zhu, H. Ju, *Adv. Funct. Mater.* **2013**, *23*, 2422.
[25] J. Shen, Y. Hu, C. Li, C. Qin, M. Ye, *Small* **2009**, *5*, 82.
[26] G. He, J. Zhao, S. Hu, L. Li, Z. Li, Y. Li, Z. Li, H. Wu, X. Yang, Z. Jiang, *ACS Appl. Mater. Interfaces* **2014**, *6*, 15291.
[27] M. Fang, K. Wang, H. Lu, Y. Yang, S. Nutt, *J. Mater. Chem. A* **2009**, *19*, 7098.
[28] Y.-S. Ye, Y.-N. Chen, J.-S. Wang, J. Rick, Y.-J. Huang, F.-C. Chang, B.-J. Hwang, *Chem. Mater.* **2012**, *24*, 2987.
[29] B. Li, W. Hou, J. Sun, S. Jiang, L. Xu, G. Li, M. A. Memon, J. Cao, Y. Huang, C. W. Bielawski, J. Geng, *Macromolecules* **2015**, *48*, 994.
[30] F. Beckert, A. M. Rostas, R. Thomann, S. Weber, E. Schleicher, C. Friedrich, R. Mülhaupt, *Macromolecules* **2013**, *46*, 5488.
[31] a) T. Ramanathan, A. A. Abdala, S. Stankovich, D. A. Dikin, M. Herrera-Alonso, R. D. Piner, D. H. Adamson, H. C. Schniepp, X. Chen, R. S. Ruoff, S. T. Nguyen, I. A. Aksay, R. K. Prud'Homme, L. C. Brinson, *Nat. Nanotechnol.* **2008**, *3*, 327; b) K. Hu, D. D. Kulkarni, I. Choi, V. V. Tsukruk, *Prog. Polym. Sci.* **2014**, *39*, 1934.
[32] G. He, L. Nie, X. Han, H. Dong, Y. Li, H. Wu, X. He, J. Hu, Z. Jiang, *J. Power Sources* **2014**, *259*, 203.
[33] Y. G. Jin, S. Z. Qiao, J. C. D. daCosta, B. J. Wood, B. P. Ladewig, G. Q. Lu, *Adv. Funct. Mater.* **2007**, *17*, 3304.
[34] J. Zhao, Y. Zhu, F. Pan, G. He, C. Fang, K. Cao, R. Xing, Z. Jiang, *J. Membr. Sci.* **2015**, *487*, 162.
[35] H. Li, Z. Song, X. Zhang, Y. Huang, S. Li, Y. Mao, H. J. Ploehn, Y. Bao, M. Yu, *Science* **2013**, *342*, 95.
[36] D. A. Dikin, S. Stankovich, E. J. Zimney, R. D. Piner, G. H. Dommett, G. Evmenenko, S. T. Nguyen, R. S. Ruoff, *Nature* **2007**, *448*, 457.
[37] T. J. Peckham, S. Holdcroft, *Adv. Mater.* **2010**, *22*, 4667.
[38] L. Wu, Z. Zhang, J. Ran, D. Zhou, C. Li, T. Xu, *Phys. Chem. Chem. Phys.* **2013**, *15*, 4870.
[39] D. S. Liu, J. N. Ashcraft, M. M. Mannarino, M. N. Silberstein, A. A. Argun, G. C. Rutledge, M. C. Boyce, P. T. Hammond, *Adv. Funct. Mater.* **2013**, *23*, 3087.
[40] a) R. Tayouo, G. David, B. Améduri, J. Rozière, S. P. Roualdès, *Macromolecules* **2010**, *43*, 5269; b) A. Sannigrahi, S. Takamuku, P. Jannasch, *Poly. Chem.* **2013**, *4*, 4207.

[41] J. Parvole, P. Jannasch, *Macromolecules* **2008**, *41*, 3893.
[42] a) K. Hatakeyama, M. R. Karim, C. Ogata, H. Tateishi, A. Funatsu, T. Taniguchi, M. Koinuma, S. Hayami, Y. Matsumoto, *Angew. Chem. Int. Ed.* **2014**, *53*, 6997; b) M. R. Karim, K. Hatakeyama, T. Matsui, H. Takehira, T. Taniguchi, M. Koinuma, Y. Matsumoto, T. Akutagawa, T. Nakamura, S. Noro, T. Yamada, H. Kitagawa, S. Hayami, *J. Am. Chem. Soc.* **2013**, *135*, 8097; c) K. H. Yama, M. R. Karim, C. O. H. Tateishi, T. Taniguchi, M. Koinuma, S. Hayami, Y. Matsumoto, *Chem. Commun.* **2014**, *50*, 14527; d) W. Gao, G. Wu, M. T. Janicke, D. A. Cullen, R. Mukundan, J. K. Baldwin, E. L. Brosha, C. Galande, P. M. Ajayan, K. L. More, A. M. Dattelbaum, P. Zelenay, *Angew. Chem. Int. Ed.* **2014**, *53*, 3588; e) R. Kumar, K. Scott, *Chem. Commun.* **2012**, *48*, 5584; f) Y. Liu, S. Liu, X. Lai, J. Miao, D. He, N. Li, F. Luo, Z. Shi, S. Liu, *Adv. Funct. Mater.* **2015**, *25*, 4480.
[43] B. Wu, J. Pan, L. Ge, L. Wu, H. Wang, T. Xu, *Sci. Rep.* **2014**, *4*, 4334.
[44] a) B. G. Choi, J. Hong, Y. C. Park, D. H. Jung, W. H. Hong, P. T. Hammond, H. Park, *ACS Nano* **2011**, *5*, 5167; b) H. W. Kim, H. W. Yoon, S. M. Yoon, B. M. Yoo, B. K. Ahn, Y. H. Cho, H. J. Shin, H. Yang, U. Paik, S. Kwon, J. Y. Choi, H. B. Park, *Science* **2013**, *342*, 91.
[45] S. J. Paddison, K. D. Kreuer, J. Maier, *Phys. Chem. Chem. Phys.* **2006**, *8*, 4530.
[46] Z. Li, G. He, B. Zhang, Y. Cao, H. Wu, Z. Jiang, Z. Tiantian, *ACS Appl. Mater. Interfaces* **2014**, *6*, 9799.
[47] G. He, Z. Li, Y. Li, Z. Li, H. Wu, X. Yang, Z. Jiang, *ACS Appl. Mater. Interfaces* **2014**, *6*, 5362.
[48] H. Zhang, P. K. Shen, *Chem. Soc. Rev.* **2012**, *41*, 2382.
[49] S. K. Nataraj, C. H. Wang, H. C. Huang, H. Y. Du, S. F. Wang, Y. C. Chen, L. C. Chen, K. H. Chen, *ChemSusChem* **2012**, *5*, 392.
[50] G. Li, Q. Shi, S. J. Yuan, K. G. Neoh, E. T. Kang, X. Yang, *Chem. Mater.* **2010**, *22*, 1309.
[51] K. Si, R. Wycisk, D. Dong, K. Cooper, M. Rodgers, P. Brooker, D. Slattery, M. Litt, *Macromolecules* **2013**, *46*, 422.
[52] Z. Li, Z. Jiang, H. Tian, S. Wang, B. Zhang, Y. Cao, G. He, Z. Li, H. Wu, *J. Power Sources* **2015**, *288*, 384.